Low-Power BLACK-ICE Detection for Safety Critical Edge Devices on Roads

Mohammadreza Najafi, Saeid Gorgin, Mohammad K Fallah, Jeong-A Lee
Department of Computer Engineering, Chosun University, Gwangju, South Korea
najafi@chosun.kr, gorgin@chosun.ac.kr, mkfallah@chosun.ac.kr, jalee@chosun.ac.kr

***Abstract*—The technological advancements in video surveillance systems represent a modern, secure, and sustainable infrastructure for smart cities. Nevertheless, detecting anomalous events in surveillance footage remains challenging, often necessitating considerable human intervention. A notable anomaly with severe implications is the presence of BLACK-ICE on highway surfaces. The presence of BLACK-ICE renders the road slippery, heightening the risk of safety incidents for pedestrians and vehicles. Notably, identifying BLACK-ICE is challenging due to its transparent nature, distinguishing it from other slippery surfaces like wet or snowy roads. In this regard, Closed-Circuit Television (CCTV) systems deployed on roadways emerge as a valuable tool for BLACK-ICE detection. Recognizing the time-sensitive nature of anomaly detection in computer vision applications, this research specifically focuses on investigating BLACK-ICE surface detection using edge devices. A novel method based on the Convolutional Neural Network (CNN), which calculates the sharpness and glossiness factors of the road surface, has been introduced to enhance performance and optimize resource utilization without compromising accuracy.**

***Index Terms*—Road Safety, BLACK-ICE Detection, CCTV, Machine Learning, Sharpness and Glossiness.**

I. Introduction

The safety systems within smart cities play a vital role, especially considering the potential risks posed by various environmental factors. A notable anomaly on highways is the existence of icy road surface conditions, where annually in the United States, more than $116,800$ individuals experience injuries in vehicle accidents on icy pavements, as indicated by the Federal Highway Administration [1]. Beyond the hazards posed by icy conditions, BLACK-ICE is identified as an even more difficult situation, frequently leading to accidents. The collision involving 69 vehicles on the Virginia Expressway in December 2019 and a traffic incident on the Yeongcheon Expressway in Korea during the same month were attributed to the presence of BLACK-ICE [2]. The incidents resulting in casualties from BLACK-ICE accidents persist on a global scale. Various preventive measures, including the proposal of initiatives such as the installation of grooving, the deployment of LED signs, and the implementation of heat wires on road surfaces, are currently under consideration . However, given that these measures are not preemptive, efforts are underway to formulate a proactive strategy to prevent BLACK-ICE accidents.

Identifying BLACK-ICE is challenging for drivers, creating unsafe situations [2]. Even though some advanced sensors exist for BLACK-ICE detection, they have some potential and challenges. Table I illustrates a compilation of prevalent sensors utilized for ice detection, accompanied by their respective detection methodologies and associated challenges. Even though Contact sensors [3], IR sensors [4], and Optical sensors [5] have high accuracy in detecting icy roads surfaces, their substantial installation costs is a big challenge. On the other hand, the most common sensor is the camera, while its sensitivity in low-light conditions holds significance. Therefore, it is noteworthy that the impact of low-light conditions in deployed solutions on CCTVs should be mitigated.

Video surveillance has a significant application of CV, extensively utilized in both public and private settings for observation and monitoring purposes . Intelligent video surveillance systems are deployed to autonomously identify, monitor, and analyze entities at an advanced level, eliminating the need for human intervention [7]. The increasing deployment of surveillance cameras in public spaces, including roadways, intersections, and shopping centers, aims to enhance public safety [8]. However, the monitoring capacities of law enforcement organizations have not kept pace, resulting in a noticeable disparity in camera usage, rendering the camera-to-human monitor ratio unsustainable [9].

This paper introduces an innovative method to reuse the existing infrastructures with significant potential as a cost-effective and tolerant solution applicable to diverse cold-climate scenarios. In this regard, a Fully Convolutional Neural Network (FCNN) is utilized to extract the Region Of Interest (ROI) mask by detecting the road surface. Employing the resultant ROI as the input for the classifier markedly reduces computational load, concurrently elevating accuracy. After identifying the ROI geometry, a MobileNet classification model is employed to classify images as ICE or NOT-ICE, while BLACK-ICE falls under the space between these two categories. In addition, we introduced a novel formula called the BLACK-ICE factor, tailored to process information with heightened accuracy, addressing the complexities associated

TABLE I
SUMMARY OF EXISTING SENSOR DEVICES USED IN BLACK-ICE DETECTION.

Sensor Name	BLACK-ICE Detection Method	Main Challenge
Contact sensors [3]	Temperature and humidity estimations to verify conditions conducive to black ice formation	Complexity of managing distributed sensors Substantial installation costs
IR sensors [4] Optical sensors [5]	Leveraging absorption coefficients that vary with wavelength	Susceptibility to sunlight interference Substantial installation costs
Cameras [2], [6]	Vision-based approach to detect black ice on road surfaces	Susceptibility to low light conditions

with uncertainty in the determination between BLACK-ICE and NOT-ICE. The empirical findings in our investigation reveal the capacity to identify BLACK-ICE with a precision rate of 98.6%. Additionally, the processing time of each frame is 10.8 milliseconds with power consumption of 10.23 watts. These results underscore the efficacy of our algorithm in achieving real-time and dependable BLACK-ICE detection, particularly when deployed on edge devices.

II. PRELIMINARIES AND BACKGROUND

A. HSV Image Format

The HSV color space is designed to mimic human's interpretation of colors by representing the color information into Hue, Saturation, and Value components. Hue represents the type of color, such as red, green, or blue. It is measured in degrees on a color wheel, where 0 and 360 correspond to red, 120 to green, and 240 to blue. The circular nature of the hue scale reflects the continuous spectrum of colors. Saturation refers to the intensity or vividness of a color. A saturation value of 0 results in a grayscale image, while higher values represent more vibrant colors. Saturation is typically normalized to a scale between 0 and 1. The value represents the brightness or lightness of a color. The 0 value corresponds to black, and 1 corresponds to white. Intermediate values determine the intensity of the color.

B. Sharpness and Glossiness

Sharpness refers to the clarity and detail in an image [10]. A sharp image has well-defined edges and fine details. Glossiness refers to the perception of shininess or reflective quality in an image [11]. It is the property of a surface to reflect light in a specular (mirror-like) manner. Glossiness is often associated with the material and lighting conditions in a scene.

C. MobileNet

MobileNet is a family of neural network architectures designed for efficient and lightweight deep learning on mobile and embedded devices [12]. The MobileNet architecture is flexible and can be customized to different computational budgets by adjusting hyperparameters. This adaptability makes it suitable for different applications, including image classification, object detection, and semantic segmentation, particularly in environments with limited computational resources including edge devices and IoT devices.

III. PROPOSED METHOD

The proposed method unfolds in two phases: ROI mask extraction and BLACK-ICE detection. The initial phase is executed only once per camera view; thus, its computational expense remains separate from real-time processing. Subsequently, the second phase encompasses the real-time analysis of road surface and the detection of possible danger.

A. Phase I: ROI Mask Extraction

This phase consists of the ROI mask determination which occurs as a one-time process for each CCTV system, maintaining a fixed viewpoint. To this end, we employed an FCNN, which represents an adapted model based on CNN and is renowned for its efficacy in image classification. FCNN demonstrates proficiency in learning to delineate the road surface area within input images [9]. Comprising three segments, including an encoder (consisting of a pre-trained model and 1-by-1 convolutions) and a decoder (involving transposed convolutions), FCNN exhibits notable performance. We served a VGG16 trained on the ImageNet dataset as the encoder. Notably, its 1-by-1 convolution layer is substituted with a fully-connected layer. The decoder incorporates transposed convolution layers to upsample the input, restoring it to its original size.

Figure 1(a) presents the input image. We denote it by $x \subset \mathcal{N}^{C \times H \times W}$, where C, H, and W indicate the number of input channels and the image height and width, respectively. The FCNN extracts the ROI identifying the road surface, as shown in Fig.1(b). Following this, Fig.1(c) presents its corresponding ROI mask M. Through the cropping of the input image using M, a masked image $x' \subseteq x$ is produced. Also, M remains constant for each CCTV system, computed only once and stored in the embedded memory. During the inference phase, it is retrieved from the memory, incurring no computational load. In addition, ROI acts to narrow down the processing area, optimizing the search for a solution and concurrently reducing overall power consumption. The focused processing not only minimizes PT, moving towards real-time problem-solving but also contributes to efficiency gains by excluding irrelevant points from processing, ultimately leading to a reduction in overall power consumption.

B. Phase II: BLACK-ICE Detection

The primary objective of this phase is to detect the BLACK-ICE while enhancing the performance and concurrently reducing energy consumption and resource utilization compared to

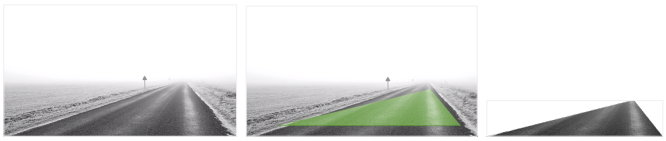

(a) (b) (c)

Fig. 1. The steps of generating ROI by the FCNN model. (a)The input image x. (b)Overlaying the ROI mask M with x. (c)The masked ROI x'.

contemporary methods. In this regard, this section delineates our algorithm and the implementation for calculating the likelihood of the existence of BLACK-ICE in the masked image x'. Initially, we constructed a dataset comprising road surface images, categorized into two classes: ICE and NOT-ICE. In this classification, images containing BLACK-ICE are designated under the ICE category. For the classification of the input image x', we conduct training on the MobileNet-V2 model using our generated dataset, which generates from [13] dataset images. This model predicts the likelihood of x' for the ICE class, denoted as $y_{ice} \in [0, 1]$, and can be parameterized as Equation (1).

$$y_{ice} = \mathcal{M}(\Theta, x') \tag{1}$$

where, $\mathcal{M}$ is tne computational mode (MobileNet-v2) and Θ is the model parameters. Of course, for each input image x', the MobileNet-v2 generates two values $y_{ice}, \bar{y}_{ice} \epsilon [0, 1]$, which represent the ICE likelihood and NOT-ICE likelihood, respectively. Since $y_{ice} + \bar{y}_{ice} = 1$, we omit $\bar{y}_{ice}$ in the presentation. Then, the sharpness factor $\mathcal{S}$ [14] of x' is calculated according to the gradient of the image by Equation (2).

$$\mathcal{S} = \frac{1}{|x'|} \sum_{i \in x'} \sqrt{\left(\frac{\partial \mathcal{I}_i}{\partial w_i}\right)^2 + \left(\frac{\partial \mathcal{I}_i}{\partial h_i}\right)^2} \tag{2}$$

where, $|x'|$ is the total number of pixels in x', $\mathcal{I}_i \in [0, 255]$ indicates the intensity of the pixel i, and (w_i, h_i) is its position in the image x'. As well, the intensity $\mathcal{I}_i$ for each pixel i of an HSV image is approximately calculated by Equation (3), where H_i, S_i and V_i are the corresponding Hue, Saturation, and Value parameters, respectively.

$$\mathcal{I}_i \simeq 0.299 \times H_i + 0.587 \times S_i + 0.114 \times V_i \tag{3}$$

In Equation (2) the $\frac{\partial \mathcal{I}_i}{\partial w_i}$ and $\frac{\partial \mathcal{I}_i}{\partial h_i}$ are the partial derivatives of intensity with respect to w_i and h_i, representing the gradients in the horizontal and vertical directions. The glossiness is intricately linked to how light interacts with the surfaces depicted in an image. In the endeavor to quantify glossiness, we engage in the computation of local contrast. This process entails determining the standard deviation of pixel intensities within defined localized regions which is served as a metric for assessing contrast. The glossiness factor g_i [15] of pixel i located in (w_i, h_i) position can be estimated utilizing Equation (4).

$$g_i = \sqrt{\frac{1}{|N_i|} \sum_{j \in N_i} \left(\mathcal{I}_j - \bar{\mathcal{I}}_i\right)^2} \tag{4}$$

where, N_i denotes the set of neighboring pixels of pixel i, $\mathcal{I}_j$ represents the intensity of the pixel situated at the position (w_j, h_j) in the image x'. Also, $\bar{\mathcal{I}}_i$ signifies the average intensity of all the pixels in N_i. The comprehensive glossiness factor for an entire image can be approximated through Equation (5).

$$\mathcal{G} \simeq \mathbb{E}_{\ i \in x'} \left[g_i\right] \tag{5}$$

For the computation of Sharpness and Glossiness factors $\mathcal{S}$ and $\mathcal{G}$, the HSV representation of the input image x' is employed. This choice was motivated by the inherent advantages of HSV, where the manipulation of overall image brightness while preserving color information is more straightforward compared to the RGB representation. As delineated by Equations (1) to (5), the parameters $\mathcal{G}$, $\mathcal{S}$, and y_{ice} exhibit mutual independence, enabling concurrent computation during the inference phase. In the end, the detection of differences between ICE and BLACK-ICE is achieved through the equation 6, while the identification of NOT-ICE, representing a normal road surface, is facilitated by the presence of y_{ice}.

$$\omega = \mathcal{G} \times \mathcal{S} \tag{6}$$

We have introduced a novel equation to calculate a unique parameter known as the BLACK-ICE Factor, expressed in Equation 9. In Equation 9, the parameter ν and μ are computed using Equation 7, 8 where α and φ represent the hyperparameter. Additionally, $\wedge$ corresponds to the logical "and" operation.

$$\nu = \begin{cases} 0 & if \quad y_{ice} < \alpha \\ 1 & if \quad y_{ice} \geq \alpha \end{cases} \tag{7}$$

$$\mu = \begin{cases} 0 & if \quad \omega < \varphi \\ 1 & if \quad \omega \geq \varphi \end{cases} \tag{8}$$

$$\mathcal{B} = \mu \wedge \nu \tag{9}$$

Figure 2 illustrates three categories of road surfaces in RGB format and their corresponding HSV images. The values of $\mathcal{G}$, $\mathcal{S}$, ω and y_{ice} as well as the corresponding BLACK-ICE Factor $\mathcal{B}$ for the HSV images are detailed in Table II. Significantly, the average value of ω for 100 images classified as BLACK-ICE is $\mathbf{1719.12}$, demonstrated as AVG_{BI}. Also, this average for 100 ICE images that are not BLACK-ICE is $\mathbf{118.81}$, demonstrated as AVG_{WI}. The difference between AVG_{BI} and AVG_{WI} provides a reasonable basis to conclude that if ω exceeds the threshold of 1000, the model classifies x' as BLACK-ICE, suggesting that setting φ to 1000 is advisable. Moreover, as illustrated in Table II, while there exists a notable distinction in ω for NOT-ICE and BLACK-ICE, relying solely on ω for BLACK-ICE detection is insufficient. This is because ω can only accentuate the disparity between BLACK-ICE and ICE, and the significance of ν is crucial for NOT-ICE diagnosis. Algorithm 1 presents the general procedure of our proposed method described in this section.

(a) (b) (c) (d) (e) (f)

Fig. 2. Three road surfaces in RGB format with their corresponding HSV format. (a) RGB format for NOT-ICE. (b) RGB format for ICE. (c) RGB format for BLACK-ICE. (d) HSV format for NOT-ICE. (e) HSV format for ICE. (f) HSV format for BLACK-ICE.

TABLE II
THE VALUES OF $\mathcal{G}$, $\mathcal{S}$, y_{ice}, AND $\mathcal{B}$ FOR FIG.2 IMAGE. AVG_{BI} AND AVG_{WI} REPRESENT THE AVERAGE OF THE PARAMETERS FOR 100 IMAGES FOR BLACK-ICE AND ICE (NOT BLACK-ICE) CATEGORIES.

Category	$\mathcal{S}$	$\mathcal{G}$	y_{ice}	ω	$\mathcal{B}$
BLACK-ICE	25.34	84.76	0.84	2147.81	1
ICE	4.97	14.85	0.96	73.80	0
NOT-ICE	30.24	8.49	0.13	256.73	0
AVG_{BI}	27.21	63.18	0.85	1719.12	1
AVG_{WI}	6.77	17.55	0.93	118.81	0

Algorithm 1 BLACK-ICE Detection.

Inputs: x (Input image), M (ROI mask), Θ (MobileNet parameters), α and φ (hyperparameters)
Output: BLACK-ICE existence label
$x' \leftarrow M(x)$
begin parallel_section
  $y_{ice} \leftarrow \mathcal{M}(\Theta, x')$
  $\mathcal{S} \leftarrow Equation\ 2$
  $\mathcal{G} \leftarrow Equation\ 5$
end parallel_section
$\omega \leftarrow Equation\ 6$
$\nu \leftarrow Equation\ 7$
$\mu \leftarrow Equation\ 8$
$\mathcal{B} \leftarrow Equation\ 9$
if $\mathcal{B} == 0$ **then**
  return Not BLACK-ICE
else
  return "BLACK-ICE"
end

IV. EVALUATION AND DISCUSSION

This section assesses and contrasts our suggested approach with the most effective state-of-the-art approaches. The proposed algorithm is implemented and executed on a Mini-PC Intel® NUC Core™ i5-1145G7 Processor with 8 MB Cache, 16 GB DDR4 RAM, and 4.4 GHz frequency.

A. Experimental Setup

In the initial phase of our experimentation, we first train the FCNN model to acquire the road mask, denoted as M. This mask is subsequently stored in embedded memory for the inference phase. The training process involved utilizing the KITTI Road dataset [16], comprising 508 images designed for road and lane estimation. These images were formatted in a bird's-eye-view perspective, with a 128×128 pixels resolution. Specifically, 384 images were designated for the training section, while the remaining 124 images constituted the test set. The FCNN underwent training with 100 epochs, a batch size of 8, and a learning rate of 0.001, ultimately achieving a commendable test accuracy of 87.3%.

In the next step, we trained the MobileNet-v2 model parameters, Θ, according to the hyperparameters detailed in Table IV and the datasets presented in [13]. The distribution of images in each category is outlined in Table III, and the BLACK-ICE images are encompassed within the ICE category. The MobileNet model demonstrated a high accuracy of 97.8% in classifying ICE and NOT-ICE images on the test images.

The proposed algorithm underwent rigorous testing on three types of datasets, which we refer to as *TYPE I*, *TYPE II*, and *TYPE III*. Besides, *TYPE I* comprises 50 ICE images and 20 BLACK-ICE images, serving the sole purpose of assessing the accuracy in detecting BLACK-ICE from ICE images through the utilization of glossiness and sharpness factors. Also, *TYPE II* consists of 50 ICE images, 20 BLACK-ICE images, and an additional 80 NOT-ICE images, aimed to evaluate the accuracy and PT of BLACK-ICE detection using MobileNet and BLACK-ICE factor $\mathcal{B}$. Additionally, *TYPE III* mirrors the image quantity and category distribution of *TYPE II*, differs in that the images contain additional details beyond the road surface for analyzing the effects of M on the accuracy, PT, and power usage. *TYPE III* is employed to gauge the accuracy and PT of the proposed algorithm outlined in Algorithm 1. For *TYPE III* dataset, a road surface mask M was computed and stored for each image. Subsequently, in the ensuing subsection, we compare our proposed algorithm's accuracy and power usage with other vision-based models, ultimately reporting on the observed PT.

TABLE III
GENERATED DATASET FOR TRAINING THE MOBILNET-V2 MODEL. BLACK-ICE IMAGES ARE ENCOMPASSED WITHIN THE ICE CATEGORY.

Category	*# Train*	*# Test*
ICE	250	50
BLACK-ICE	70	10
NOT-ICE	320	60

TABLE IV
THE HYPERPARAMETERS OF MOBILENET-V2.

Hyperparameter	*Value*
Width Multiplier	1.0
Resolution Multiplier	1.0
Depthwise Separable Convolution	Yes
Initial Number of Filters	32
Expansion Factor	6
Dropout Rate	0.2
Activation Function	ReLU
Number of Classes	2
Batch Size	16
Number of Epochs	100

B. Discussion

We conduct a comparative evaluation of the model accuracy and processing time across the test datasets. As illustrated in Fig.3, the best value for α is determined to be 0.3. Additionally, it is advisable to set the value of φ to 1000.

The outcomes presented in Table V indicate that the proposed model attains a perfect accuracy of 100% in detecting BLACK-ICE in *TYPE I*. In *TYPE II*, the proposed model achieves an accuracy of 98.9%. As indicated in Table V, the accuracy of our proposed model in detecting BLACK-ICE surpasses that of the MobileNet-V2 model (97.8%). This improvement is attributed to cases where BLACK-ICE images are potentially misclassified as NOT-ICE by MobileNet-V2. Our proposed algorithm (1) addresses this by detecting such images through the calculation of the BLACK-ICE factor,$\mathcal{B}$. Additionally, it is worth noting that both *TYPE II* and *TYPE I* share identical PT values, thanks to the parallel processing section of the proposed algorithm, as detailed in Table V. Lastly, in *TYPE III*, the proposed model's accuracy experiences a slight decrease (98.6%) influenced by incorporating FCNN effects. Despite this decrease, the PT of the proposed algorithm is recorded at 10.8 ms, demonstrating appropriateness for real-time processing [17]. Moreover, the macro recall and macro precision metrics for "TYPE III" are determined to be 99.16% and 96.96% respectively.

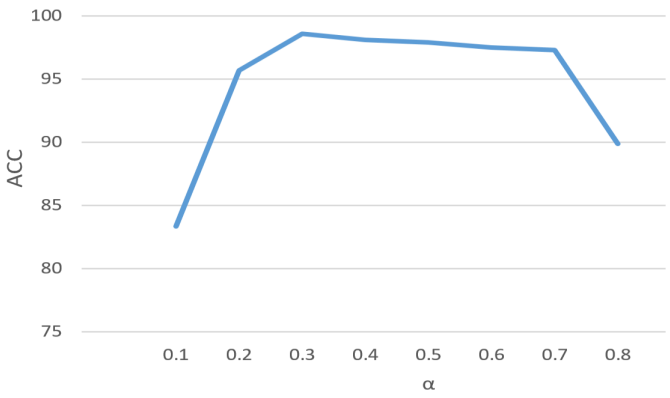

Fig. 3. The effect of α on the accuracy of the proposed model.

TABLE V
THE ACCURACY AND PROCESSING TIME OF ALGORITHM 1.

TYPE	*Accuracy%*	*Processing Time(ms)*
I	100	9.1
II	98.9	9.1
III	98.6	10.8

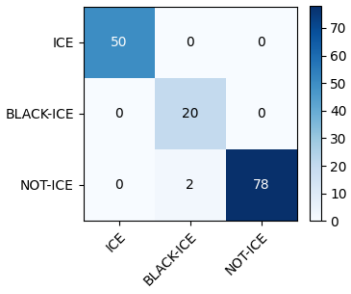

Fig. 4. The confusion matrix for *TYPE III* classification.

Figure 4 depicts the confusion matrix of the proposed method test on "TYPE III", revealing predominantly misclassifies NOT-ICE images as BLACK-ICE. This misclassification stems from errors within the FCNN and MobileNet models. According to this information, the F1-score for the ICE category in "TYPE III" stands at 100%, while for BLACK-ICE it is 95%, and for NOT-ICE it is 99%. Accordingly, from a safety standpoint, the proposed method rarely misclassifies the BLACK-ICE category, rendering it suitable for safe driving applications. As delineated in Table VI, the proposed model attains the highest level of accuracy at an impressive 98.6%. Moreover, to measure power usage, we employed the *cProfile Python* library. For the comparison, we calculated the number of MAC operations for all the models, estimating their power usage based on the relationship between the number of MAC operations and power. The proposed model demonstrates the second most economical power consumption compared to the other models under consideration, registering at 10.23 W. This observation underscores the suitability of the proposed model for operation on resource-aware devices. This improvement becomes particularly critical when deploying the proposed model on edge devices such as CCTVs and portable devices with limited resources.

TABLE VI
COMPARISON OF THE ACCURACY AND POWER CONSUMPTION OF THE PROPOSED MODEL WITH THE STATE-OF-THE-ART ON *TYPE III* DATASET.

Model	***Accuracy%***	***Power(W)***
Proposed model	**98.6**	**10.23**
CNN [2]	**98.3**	15.31
Hyperspectral + DL [18]	97	12.78
CNN [19]	95.6	13.52
CNN [20]	95	10.83
Image Analysis [21]	83	**9.74**

V. RELATED WORKS

The identification of BLACK-ICE has been investigated through diverse approaches, encompassing sensor-based methods [22], sound wave utilization [23], [24], and the application of light sources [25]. Tabatabai and Aljuboori [22], [26] focused on BLACK-ICE, ice, and water detection on roads and bridges, employing sensors embedded within concrete. Their proposed sensor, based on alterations in electrical resistance between stainless steel columns inside the concrete, proved effective in detecting road surface conditions, offering the potential for accident prevention. Additionally, Alimasi et al [27] designed a BLACK-ICE detector using an optical sensor and an infrared thermometer. Abdalla et al [26] introduced a Kinect-based system for BLACK-ICE detection, including classifying various ice types, thickness, and volume measurements. They achieved high accuracy in denoting ice within a specific camera range, with a low error rate in measured thickness and volume. Ma and Ruan [25] investigated a BLACK-ICE detection method utilizing three-wavelength non-contact optical technology. Employing wavelengths (1310 nm, 1430 nm, 1550 nm), they differentiated dry, wet, BLACK-ICE,

ice, and snowy conditions. Their study successfully detected BLACK-ICE through each wavelength's reflectance, laying the groundwork for potential equipment development in road condition detection. Kim et al [19] utilized Range-FFT results obtained by the mmWave sensor for BLACK-ICE detection, with accuracy dependent on the surface's smoothness or roughness. Furthermore, Lee et al [2] employed CNNs for BLACK-ICE detection using camera images. Despite achieving high accuracy through deep learning, this approach incurred increased computational operations and subsequent higher power consumption.

VI. Conclusion

The primary objective of this research is the development of an efficient algorithm for BLACK-ICE detection in CCTV images, emphasizing considerations of accuracy and resource efficiency tailored for edge devices. At first, an FCNN generates the ROI mask according to each camera view, emphasizing the road surface. This strategy reduces computational load and diminishes power consumption when executing on resource-aware edge devices. In the following, a MobileNet-V2 model is trained to classify the ROI region into either ICE or NOT-ICE categories. Simultaneously, Glossiness and Sharpness factors are computed for this region. In addition, we introduced a BLACK-ICE factor ($\mathcal{B}$) based on the Glossiness, Sharpness, and ICE likelihood calculated by the MobileNet model to identify instances of BLACK-ICE. The presented algorithm showcased an accuracy level of 98.6% with a power consumption of 10.23 W, reflecting a significant reduction of 33% in power usage and superior accuracy compared to current vision-based models. This comprehensive approach integrates multiple image analysis techniques, contributing to a robust solution for real-time BLACK-ICE detection in surveillance scenarios.

Acknowledgment

This study was supported by a research fund from Chosun University, K949856045.

References

[1] Snow & ice road weather management [accessed 29-11-2023], https://ops.fhwa.dot.gov/weather.

[2] H. Lee, M. Kang, J. Song, K. Hwang, The detection of black ice accidents for preventative automated vehicles using convolutional neural networks, Electronics 9 (12) (2020) 2178.

[3] T. Liu, Q. Pan, J. Sanchez, S. Sun, N. Wang, H. Yu, Prototype decision support system for black ice detection and road closure control, IEEE Intelligent Transportation Systems Magazine 9 (2) (2017) 91–102.

[4] Y. Nakanishi, Y. Kushihi, Black-ice and standing-water detection system, uS Patent App. 16/647,046 (Dec. 2 2021).

[5] X. Ma, C. Ruan, Method for black ice detection on roads using tri-wavelength backscattering measurements, Applied Optics 59 (24) (2020) 7242–7246.

[6] C. H. Crawford, S. Daijavad, J. A. Gunnels, T. Nowicki, G. M. Swirszcz, J. Xenidis, Method for black ice detection and prediction, uS Patent 9,940,549 (Apr. 10 2018).

[7] A. C. Davies, S. A. Velastin, A progress review of intelligent cctv surveillance systems, Proc. IEEE IDAACS (2005) 417–423.

[8] M. P. Ashby, The value of cctv surveillance cameras as an investigative tool: An empirical analysis, European Journal on Criminal Policy and Research 23 (3) (2017) 441–459.

[9] N. Mohammadreza, S. Gorgin, D. Javaheri, J.-A. Lee, Ice detection on edge device based on most significant digit first svm, in: Proceedings of the 2022 6th International Conference on Video and Image Processing, 2022, pp. 61–66.

[10] D. Shaked, I. Tastl, Sharpness measure: Towards automatic image enhancement, in: IEEE International Conference on Image Processing 2005, Vol. 1, IEEE, 2005, pp. I–937.

[11] A. C. Chadwick, R. Kentridge, The perception of gloss: A review, Vision research 109 (2015) 221–235.

[12] A. G. Howard, M. Zhu, B. Chen, D. Kalenichenko, W. Wang, T. Weyand, M. Andreetto, H. Adam, Mobilenets: Efficient convolutional neural networks for mobile vision applications, arXiv preprint arXiv:1704.04861 (2017).

[13] T. Zhao, Y. Wei, Road surface image dataset with detailed annotations (2022). doi:10.17632/w86hvkrzc5.2.

[14] C. Feichtenhofer, H. Fassold, P. Schallauer, A perceptual image sharpness metric based on local edge gradient analysis, IEEE Signal Processing Letters 20 (4) (2013) 379–382.

[15] H. KUGISAWA, T. AIDA, M. EBATA, Method for measuring glossiness of spherical surfaces utilizing brightness pattern of image, IEICE Transactions on Fundamentals of Electronics, Communications and Computer Sciences 74 (9) (1991) 2655–2662.

[16] J. Fritsch, T. Kuehnl, A. Geiger, A new performance measure and evaluation benchmark for road detection algorithms, in: International Conference on Intelligent Transportation Systems (ITSC), 2013.

[17] Z. Chen, W. Hu, J. Wang, S. Zhao, B. Amos, G. Wu, K. Ha, K. Elgazzar, P. Pillai, R. Klatzky, et al., An empirical study of latency in an emerging class of edge computing applications for wearable cognitive assistance, in: Proceedings of the Second ACM/IEEE Symposium on Edge Computing, 2017, pp. 1–14.

[18] C. Bhattacharyya, S. Kim, Black ice classification with hyperspectral imaging and deep learning, Applied Sciences 13 (21) (2023) 11977.

[19] J. Kim, E. Kim, D. Kim, A black ice detection method based on 1-dimensional cnn using mmwave sensor backscattering, Remote Sensing 14 (20) (2022) 5252.

[20] M. Ahmad, A. M. Khan, M. Mazzara, S. Distefano, M. Ali, M. S. Sarfraz, A fast and compact 3-d cnn for hyperspectral image classification, IEEE Geoscience and Remote Sensing Letters 19 (2022) 1–5. doi:10.1109/LGRS.2020.3043710.

[21] P. Pil-won, H. Seong-su, Study on black ice detection method through color image analysis, JOURNAL OF PLATFORM TECHNOLOGY 9 (4) (2021) 90–96.

[22] H. Tabatabai, M. Aljuboori, A novel concrete-based sensor for detection of ice and water on roads and bridges, Sensors 17 (12) (2017) 2912.

[23] R. Minullin, R. Mustafin, Y. V. Piskovatskii, S. Vedernikov, I. Lavrent'Ev, A detection technique for black ice and frost depositions on wires of a power transmission line by location sounding, Russian Electrical Engineering 82 (10) (2011) 541–543.

[24] D. Gailius, S. Jačėnas, Ice detection on a road by analyzing tire to road friction ultrasonic noise, Ultragarsas/Ultrasound 62 (2) (2007) 17–20.

[25] X. Ma, C. Ruan, Method for black ice detection on roads using tri-wavelength backscattering measurements, Applied Optics 59 (24) (2020) 7242–7246.

[26] Y. E. Abdalla, M. T. Iqbal, M. Shehata, Black ice detection system using kinect, in: 2017 IEEE 30th Canadian Conference on Electrical and Computer Engineering (CCECE), IEEE, 2017, pp. 1–4.

[27] N. ALIMASI, S. TAKAHASHI, H. ENOMOTO, Development of a mobile optical system to detect road-freezing conditions, Bulletin of Glaciological Research 30 (2012) 41–51.